sors. The performance of the mesowire array–based sensors documented here challenges existing H_2 sensing technologies. In particular, mesowire array–based H_2 sensors possess four attributes: (i) fast response; (ii) room-temperature operation; (iii) diminutive power requirements of less than 100 nW; and (iv) resistance to poisoning by reactive gases, including O_2, CO, and CH_4.

References and Notes

1. C. Z. Li, H. X. He, A. Bogozi, J. S. Bunch, N. J. Tao, *Appl. Phys. Lett.* **76**, 1333 (2000); C. Z. Li, H. Sha, N. J. Tao, *Phys. Rev. B* **58**, 6775 (1998); A. Bogozi *et al.*, *J. Am. Chem. Soc.* **123**, 4585 (2001).
2. P. G. Collins, K. Bradley, M. Ishigami, A. Zettl, *Science* **287**, 1801 (2000).
3. A. Zahab, L. Spina, P. Poncharal, C. Marliere, *Phys. Rev. B* **62**, 10000 (2000).
4. J. Kong, H. J. Dai, *J. Phys. Chem. B* **105**, 2890 (2001); J. Kong *et al.*, *Science* **287**, 622 (2000).
5. Mesoscopic structures are characterized by a length scale ranging from tens of nanometers to micrometers.
6. F. A. Lewis, *The Palladium Hydrogen System* (Academic Press, New York, 1967).
7. M. P. Zach, K. Ng, R. M. Penner, *Science* **290**, 2120 (2000).
8. Details of the deposition conditions and electron diffraction characterization are available on *Science* Online at www.sciencemag.org/cgi/content/full/293/5538/2227/DC1
9. During hydrogen absorption into the nanowire, the diffusion coefficient will increase from a value characteristic of the α phase ($D_\alpha = 1.6 \times 10^{-7}$ cm^2 s^{-1}) to the β-phase value ($D_\beta = 5 \times 10^{-6}$ cm^2 s^{-1}) (6).
10. AFM measurements of palladium nanowires in functioning sensors have also been carried out. Reversible gap opening and closing is also observed in these nanowires, but the nanowire diameter can not be accurately measured because these wires are embedded in the cyanoacrylate film.

11. This work was funded by the NSF (grant CHE-0111557) and the Petroleum Research Fund of the American Chemical Society (grant 33751-AC5). R.M.P. acknowledges the financial support of the A. P. Sloan Foundation Fellowship and the Camille and Henry Dreyfus Foundation. F.F. acknowledges funding through NATO. Finally, donations of graphite by A. Moore of Advanced Ceramics are gratefully acknowledged.

6 June 2001; accepted 7 August 2001

Changes in Seismic Anisotropy After Volcanic Eruptions: Evidence from Mount Ruapehu

Vicki Miller* and Martha Savage†

The eruptions of andesite volcanoes are explosively catastrophic and notoriously difficult to predict. Yet changes in shear waveforms observed after an eruption of Mount Ruapehu, New Zealand, suggest that forces generated by such volcanoes are powerful and dynamic enough to locally overprint the regional stress regime, which suggests a new method of monitoring volcanoes for future eruptions. These results show a change in shear-wave polarization with time and are interpreted as being due to a localized stress regime caused by the volcano, with a release in pressure after the eruption.

The prediction of volcanic eruptions is one of the primary goals of hazards research. Changes in stress indicators would be particularly useful in understanding the buildup of stress and strain before an eruption. One suggested method of monitoring stress is to observe changes in shear-wave splitting. Shear-wave splitting occurs when elastic waves enter an anisotropic medium. The energy is split into two components, in which the component polarized in one direction travels faster than its orthogonal counterpart. Shear-wave splitting in the upper 10 to 15 km of the crust may result from fluid-filled cracks, microcracks, preferentially oriented pore space, or a combination of these factors (*1*, *2*). Differential stress preferentially closes cracks that are aligned perpendicular to the maximum principal stress. The cracks that remain open are thus aligned perpendicular to the minimum horizontal compressional stress axis. The initial polarization (the "fast direction" or ϕ) of shear-wave splitting in cracked media is parallel to the cracks and therefore to the maximum compressive stress. The time delay (δt) between the arrival of the two components depends on the path length and on the amount of anisotropy in the particular ray path direction through the material. Initial polarizations are a more robust feature than δt, which typically shows considerable scatter (*3–6*). Because of these difficulties, controversy continues as to whether changes reported in δt are caused by changes in the stress regime due to earthquakes and volcanic activity or are due simply to path differences (*3*, *4*, *7*, *8*). Slight changes of 7° to 10° in ϕ during hydraulic pumping in a hot, dry, rock geothermal reservoir were suggested (*9*), whereas temporal variations in ϕ related to tectonic and/or volcanic activity have not been reported.

Work on volcanic systems and rift zones has yielded ϕ of shear-wave splitting generally parallel to the maximum principal stress [for example, the Michoacan-Guanajuato volcanic field (*10*), Mexico; the Kilauea East Rift Zone, Hawaii; and the Phlegrean Fields (*11*), Italy]. However, studies in the Long Valley Caldera, California (*12*), and on the volcano Mount Vesuvius, Italy (*13*), yielded ϕ aligned with regional faulting rather than the local stress direction.

On the volcano Mount Ruapehu, New Zealand, ϕ and δt were determined with data from two separate deployments of broadband seismometers; the first during 1994 and the second in 1998 (*14*). The most recent large volcanic eruptions at Mount Ruapehu occurred in 1988 and 1995/96 (*15*). Local earthquakes within the shear-wave window (*16*, *17*) were analyzed. For each deployment, there are two data sets. The first contains earthquakes with a local magnitude (M_L) ≥ 3, with hypocenters deeper than 50 km. The second consists of events with depths shallower than 30 km and includes lower magnitudes (M_L 0.4 to 4.1). All seismograms were analyzed to determine the shear-wave splitting parameters ϕ and δt (*18–21*) [see (*22*) for examples of waveforms].

The average ϕ for both the shallow data sets (Fig. 1, A and B) is NW-SE. The 1994 average is (ϕ,δt) = (313° ± 7°, 0.10 ± 0.01 s). The 1998 average is (293° ± 12°, 0.10 ± 0.01 s). There is a greater variation in individual azimuths for 1998 [from 19° variation in 1994 to 47° in 1998 (*21*)].

The 1994 deep data set (Fig. 1C) average ϕ is NW-SE (324° ± 6°, 0.17 ± 0.03 s), similar to the shallow results. The deep 1998 data set (Fig. 1D) however, has an average ϕ of ENE-WSW (250° ± 14°, 0.11 ± 0.01 s); this is almost perpendicular to both the deep and shallow 1994 data sets.

The large scatter in most of the data sets may be caused by the irregular surface topography in the region. The NW-SE ϕ of the shallow data sets and the 1994 deep data sets is almost perpendicular to the maximum compressive stress axis of the surrounding Taupo Volcanic Zone (TVZ) and the alignment of the most recently active [<10,000 years ago] (*23*) vents (NNE-SSW). Two possible interpretations for the changes in ϕ are (i) changes from high to lower pore pressures or (ii) changes in crack orientations.

We interpret ϕ in 1994 as resulting from localized stress caused by the volcano, with a pressure source from a NNE-SSW–trending tabular (*24*) magma body, such as that indicated by regions of anomalously high *S*-wave attenuation or "shadowing" (*25*) (Fig. 2); the geometry of the magma body is induced by

Institute of Geophysics, Victoria University of Wellington, Wellington, New Zealand.

*Present address: Upper Hutt City Council, Private Bag 907, Upper Hutt, New Zealand.
†To whom correspondence should be addressed. E-mail: Martha.Savage@vuw.ac.nz

the WNW-ESE–oriented minimum compressive stress field of the TVZ. Similar dike orientations were observed in the nearby Tarawera rift eruption of 1886 (*26*), suggesting that such orientations may be common in the region.

In the first interpretation, elevated temperatures from a shallow magma intrusion cause the rapid sealing of permeable pathways (*27*). This and/or an increase in differential stress (*2*) results in regions of high pore pressure. Large pore-fluid pressures can induce the faster split shear-wave to be flipped, so that it is polarized perpendicular to the maximum horizontal compression, unlike the usual situation (*2*).

With the second interpretation, the tabular magma body becomes overpressured because of excess magma injection, which leads it to exert an outward pressure perpendicular to its sides at NW-SE. This localized stress regime overprints that of the TVZ, and cracks in the immediate vicinity of the volcano open in a NW-SE orientation. Crack orientations become pronounced at a differential stress of only 1×10^5 Pa (*28*), and a pressure of 2×10^8 Pa closes all the cracks (*29*). The volume of erupted material from each of the 1995/96 eruptions was on the order of 0.005 to 0.01 km^3 (*30*). This is a minimum estimate of the excess magma, because not all the magma would be ejected to the surface during an eruption. If we simplify the structure, which likely includes numerous dikes and sills, we can make a crude order-of-magnitude calculation. With a 1-km^3 magma chamber at 5 km depth beneath the crater (*31*) and an addition of 0.005 km^3 of magma, the expected pressure change using the equation (*32*) $(\Delta V/V)k = P$, where P is change in pressure, k is the bulk modulus [5.2×10^{10} Pa for rock at 5 km depth from the Preliminary Reference Earth Model (*33*)], and $(\Delta V/V)$ is the change in volume over the original volume, would be 2.6×10^8 Pa. Stress will decay as distance increases from the source by the relation (*32*) $1/R^2$, where R is the radial distance from the source. A pressure large enough to close all of the cracks could exist 0.85 km away from the edge of the source. A pressure large enough to enhance the alignment in crack orientations could exist at a distance of 50 km away from the source (*21*). Crack alignment is presumed to occur by grain-scale migration of fluids in microcracks (*2*). The timing of the alignment depends on the permeability of the surrounding rock, but estimates for applied differential stresses of 10 Mpa are measured in seconds to thousands of seconds for a reasonable range of rock permeabilities (10^{-9} to 10^{-6} Darcy) (*2*). Thus, the changes could have occurred between the eruptions in 1996 and the 1998 deployment.

In both interpretations, the strong alignment in the shallow 1994 data is a result of increased buildup in pressure associated with magma injection (Fig. 3). The variation in the shallow 1998 ϕ is interpreted as a result of stress released during the 1995/1996 eruption, causing a return to a more heterogeneous stress regime and a smaller range over which the stress causes reversed polarizations.

The average ϕ of the deep 1998 data is consistent with the maximum compressive stress axis of the TVZ and nearby results from a national study (*34*). Deep earthquakes record-

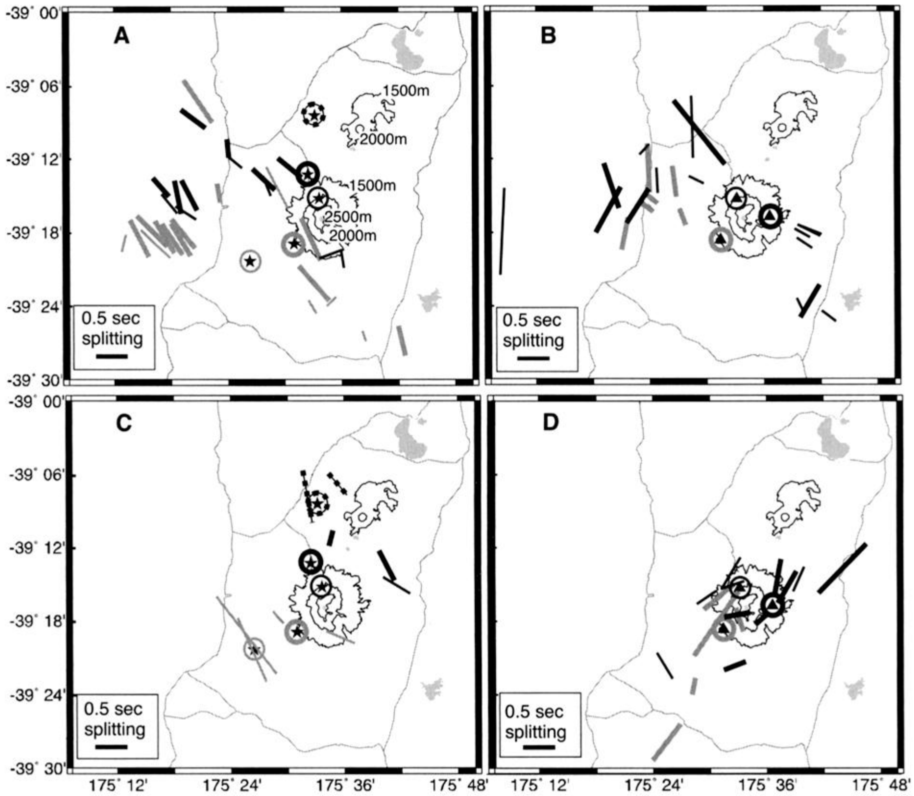

Fig. 1. Map views of Ruapehu with topographic contours shown as thin black lines and roads as thin gray lines. Irregular gray areas are lakes. The measurements are indicated by a bar whose azimuth is ϕ and whose length is proportional to δt. They are plotted at the surface projection of the point where the ray paths intersect 10 km depth. The marking of the bar corresponds to the station recording the waveform surrounded by a circle of the same marking where the measurement was recorded [stations are shown as stars in (A) and (C) (1994) and as triangles in (B) and (D) (1998)]. **(A)** Shear-wave splitting from shallow (<30 km) events recorded in 1994. **(B)** Shear-wave splitting from shallow events recorded in 1998. **(C)** Shear-wave splitting from deep (>50 km) events recorded in 1994. **(D)** Shear-wave splitting from deep events recorded in 1998.

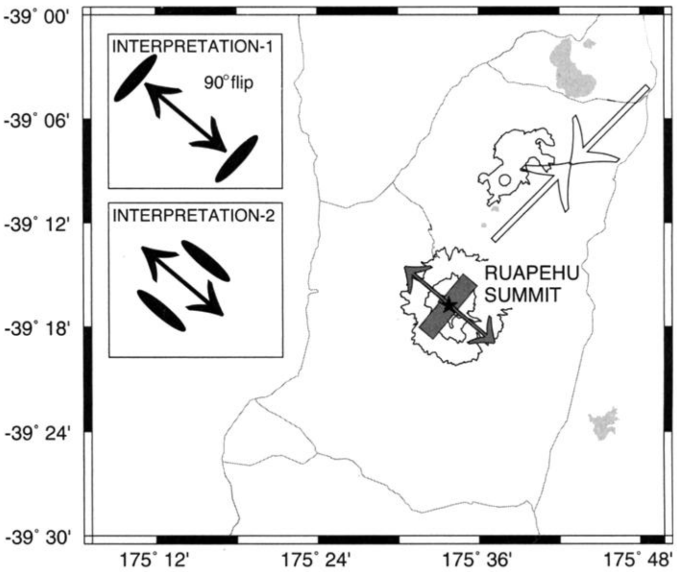

Fig. 2. Interpretation of the cause of ϕ from shallow events. The maximum compressive axis of the TVZ and alignment of the youthful vents is indicated by the white arrows. The black star marks the summit of Ruapehu, and the gray arrows represent the increased pressure from the NNE-SSW–oriented magma body, which is also shown in gray. Two interpretations are given, with the average ϕ from the shallow results indicated by the black arrows. The interpreted crack alignment is shown by the black ovals.

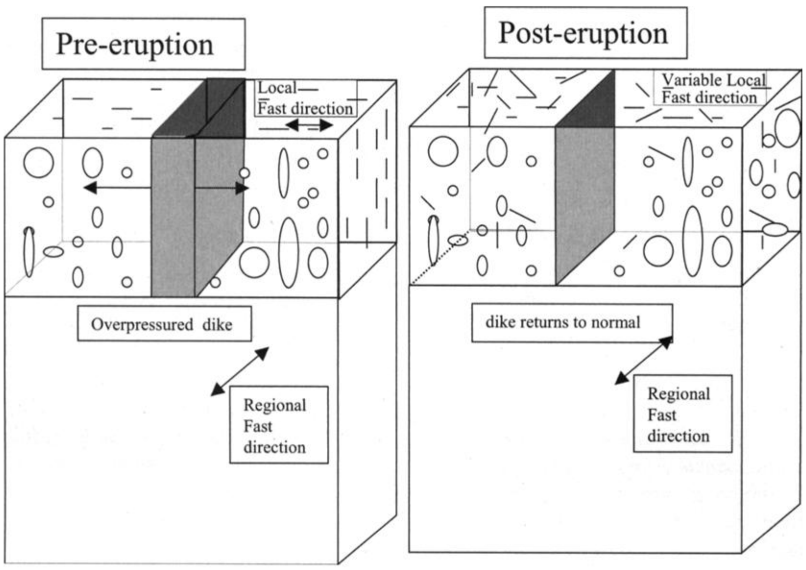

Fig. 3. Schematic cross section showing a vertical dike, which is overpressured because of magma injection before the eruption and pushes outward to close shallow cracks. After the eruption, the dike deflates and is no longer pushing outward, allowing shallow cracks to return to normal. The deeper, regional stress field remains the same in both time periods. In the real Earth, we would expect multiple dikes, but the present subsurface location of dikes is unknown.

ed during the 1994 deployment, however, have an average ϕ similar to the shallow results. The changes in ϕ cannot be due to an alignment error in seismometer deployment, as there are ϕ changes between the two 1998 data sets, and because *P*-wave polarities for both deployments indicated that the components had been aligned correctly. The ϕ for deep events recorded during 1994 may have been affected by the same factor that induced the strong alignment of ϕ for shallow events at this time, the deeper shear-wave splitting having been rotated into the NW-SE direction as it neared the surface (*6*). The release of stress in 1998 then allowed the original ϕ to be preserved.

The δt of about 0.1 s suggests small anisotropy for many of the deep paths, if the entire path contributes to the splitting. It is tempting to interpret the greater (0.17-s) splitting in 1994 as evidence for a longer path with consistent anisotropy. However, the δt's for the deep events are scattered and do not correlate with depth or distance from the earthquake (*21*). Moreover, when two standard deviations are used instead of a single standard deviation, the error bars for the deep and shallow events overlap. Heterogeneous anisotropy often yields consistent ϕ but variations in δt with changing back azimuths, which may explain the scatter in δt for the deep 1994 data (*6*). The earthquakes with most consistent δt are the shallow 1994 set. In this case, the shallowest earthquakes (at about 5 km depth) constrain anisotropy to an average of 6.4% (ranging from 0.6 to 7.2%). If the percentage anisotropy remains constant at 6.4% and the splitting reflects only the top layer of anisotropy (*6*), then the deep data sets are sampling the top 5.5 to 8.5 km of the crust.

Because the stations in the two deployments were not at identical locations, complex path effects could be causing apparent time variations. This possibility will be checked by a planned deployment to reoccupy the sites. However, the rapid lateral variations in stress or structure needed to explain the differences by path effects are less likely than the simpler explanation of a change in stress after the eruption. For example, the southwesternmost station in 1998 is less than 1 km from a 1994 station, yet at these stations the deep 1998 events have ϕ nearly perpendicular to the 1994 events, and the shallow events also have different ϕ (Fig. 1). The 0.75-s wave period corresponds to a wavelength of at least 1.5 km for a shear wave speed of 2 km/s; thus, there are differences in ϕ despite the stations being less than a wavelength apart.

Thus, the changes in shear-wave polarizations found in this study could be caused by increased magmatic pressure that either caused polarization flips in the shear wave because of increased pore pressure or that changed crack orientations. In either case, abrupt changes in shear-wave splitting polarizations may be a future indicator of volcanic activity. Shear-wave splitting may therefore become an important tool for monitoring volcanoes and predicting eruptions.

References and Notes

1. S. Crampin, *Geophys. J. Int.* **118**, 428 (1994).
2. S. V. Zatsepin, S. Crampin, *Geophys. J. Int.* **129**, 477 (1997).
3. R. C. Aster, P. M. Shearer, J. Berger, *J. Geophys. Res.* **95**, 12,449 (1990).
4. ———, *J. Geophys. Res.* **96**, 6415 (1991).
5. S. Crampin, T. Volti, R. Stefansson, *Geophys. J. Int.* **138**, F1 (1999).
6. R. L. Saltzer, J. B. Gaherty, T. H. Jordan, *Geophys. J. Int.* **141**, 374 (2000).
7. S. Peacock, S. Crampin, D. C. Booth, J. B. Fletcher, *J. Geophys. Res.* **93**, 3339 (1988).
8. S. Crampin, D. C. Booth, R. Evans, S. Peacock, J. B. Fletcher, *J. Geophys. Res.* **96**, 6403 (1991).
9. S. Crampin, S., D. C. Booth, *Sci. Drilling* **1**, 21 (1989).
10. J. R. Pacheco *et al.*, *J. South Am. Earth Sci.* **12**, 567 (1999).
11. M. K. Savage, X. R. Shih, R. P. Meyer, R. C. Aster, *Tectonophysics* **165**, 279 (1989).
12. M. K. Savage, W. A. Peppin, U. R. Vetter, *J. Geophys. Res.* **95**, 11165 (1990).
13. F. Bianco *et al.*, *Phys. Chem. Earth* (*A*) **24**, 977 (1999).
14. Nine broadband, three-component, Guralp CMG3 sensors and MARS-88 recorders were deployed from January to March 1994. Three of these instruments were deployed again from February to July 1998. The seismometer orientations are good to within $\pm 3°$.
15. S. Sherburn, C. J. Bryan, A. W. Hurst, J. H. Latter, B. J. Scott, *J. Volc. Geotherm. Res.* **88**, 255 (1999).
16. O. W. Nuttli, *Bull. Seism. Soc. Am.* **51**, 237 (1962).
17. Earthquakes incident on the free surface at an angle greater than about 35° have phase shifts even for isotropic media, due to reflections beyond the critical angle. This cone of 35° is called the shear-wave window. To determine whether the path is within this window, we use the takeoff angles of the earthquake combined with the velocity structure in the region (*35*), corrected for the local slope of the volcano (which reached a maximum of 20°).
18. We use the Seismic Analysis Code (SAC) processing package [W. C. Tapley, J. E. Tull, L. Miner, P. Goldstein, *Sac2000 Command Reference Manual Version 10.5d* (Regents of the University of California, Livermore, CA, 1992)]. We correct for instrument response then filter each event individually to ensure the best signal-to-noise ratio, using a bandpass filter ranging from 1 to 3 Hz to 1 to 10 Hz. We measure ϕ and δt with the Silver and Chan (*20*) method, grading the results using diagnostic plots (*20*). Only the highest grades are presented, so that an initial data set of 715 earthquakes within the shear-wave window was winnowed to 83 events. Reported error bars represent 1 SD. See (*22*) for examples of the waveforms.
20. P. G. Silver, W. W. Chan, *J. Geophys. Res.* **96**, 16429 (1991).
21. V. L. Miller, thesis, Victoria University of Wellington, Wellington, New Zealand (2000).
22. Supplementary Web material is available on *Science* Online at www.sciencemag.org/cgi/content/full/293/5538/2231/DC1.
23. I. A. Nairn, T. Kobayashi, M. Nakagawa, *J. Volc. Geotherm. Res.* **86**, 19 (1998).
24. T. Parsons, G. A. Thompson, *Science* **253**, 1399 (1991).
25. J. H. Latter, *J. Volc. Geotherm. Res.* **10**, 125 (1981).
26. I. A. Nairn, J. W. Cole, *N. Z. J. Geol. Geophys.* **24**, 585 (1981).
27. R. O. Fournier, *Geophys. Res. Lett.* **18**, 955 (1991).
28. S. Crampin, *Trans. R. Soc. Edinb. Earth Sci.* **89**, 121 (1998).
29. F. Hrouda, Z. Pros, J. Wohlgemuth, *Phys. Earth Planet. Int.* **77**, 251 (1993).
30. M. Nakagawa, K. Wada, T. Thordarson, C. P. Wood, J. A. Gamble, *Bull. Volcanol.* **61**, 15 (1999).
31. R. W. Hackett, thesis, Victoria University of Wellington, Wellington, New Zealand (1985).
32. T. Lay, T. T. Wallace, *Modern Global Seismology* (Academic Press, San Diego, CA, 1995), chap. 2.
33. A. M. Dziewonski, D. L. Anderson, *Phys. Earth Planet. Int.* **25**, 297 (1981).
34. E. Audoine, M. K. Savage, K. Gledhill, *J. Geophys. Res.* **105**, 8013 (2000).
35. A. W. Hurst, *Bull. Volcanol.* **60**, 1 (1998).

36. J. Neuberg, D. Francis, G. Stuart, and B. Hicks deployed the seismometers. C. Bryan and T. Hurst provided the data. Discussions with T. Hurst, R. Walcott, E. Audoine, B. Hicks, S. Crampin, and K. Gledhill helped the paper. T. Stern, J. Gamble, S. Crampin, C. Jones, and A. Sheehan reviewed an early version of the manuscript. Partial support came from grants from the New Zealand Marsden Fund and from Victoria University of Wellington.

14 June 2001; accepted 21 July 2001